Original Research *Feature article*

Conformation and protein interactions of intramolecular DNA and phosphorothioate four-way junctions

Maria Troisi, Mitchell Klein, Andrew C Smith, Gaston Moorhead, Yonatan Kebede, Raymond Huang, Elliott Parker, Hector Herrada, Elizabeth Wade, Samara Smith, Payson Broome, Jonah Halsell, Louis Estevez and Anthony J Bell Jr

Department of Chemistry and Biochemistry, University of San Diego, San Diego, CA 92110, USA
Corresponding author: Anthony J Bell Jr. Email: Anthonybell@sandiego.edu

Impact statement

This work is a step forward in the development of nucleic acid therapeutics. The design strategy put forth significantly enhances the thermostability and nuclease resistance of the resulting DNA constructs—intramolecular four-way junctions (*i*-4WJs). Three unique *i*-4WJs are assembled with phosphorothioate (PS) bonds imbedded within the junction lattice; this is the first report of PS containing 4WJs. The secondary structure of *i*-4WJs is composed of classic B- and non-standard A-form helices. This work is the first to indicate that *i*-4WJs possess A-form helices. Despite the structural perturbations, *i*-4WJs bind the target protein HMGB1 with high affinity. We believe that *i*-4WJs can serve dual roles as: (i) novel targeting reagents and (ii) a model system to evaluate the influence of nucleic acid structure (particularly A-form helices) on protein recognition. Moreover, a nucleic acid targeting strategy focused on extracellular proteins obviates the requirement for cell deliver systems that may reduce potency.

Abstract

The objectives of this study are to evaluate the structure and protein recognition features of branched DNA four-way junctions in an effort to explore the therapeutic potential of these molecules. The classic immobile DNA 4WJ, J1, is used as a matrix to design novel intramolecular junctions including natural and phosphorothioate bonds. Here we have inserted H2-type mini-hairpins into the helical termini of the arms of J1 to generate four novel intramolecular four-way junctions. Hairpins are inserted to reduce end fraying and effectively eliminate potential nuclease binding sites. We compare the structure and protein recognition features of J1 with four intramolecular four-way junctions: *i*-J1, *i*-J1(PS1), *i*-J1(PS2) and *i*-J1(PS3). Circular dichroism studies suggest that the secondary structure of each intramolecular 4WJ is composed predominantly of B-form helices. Thermal unfolding studies indicate that intramolecular four-way junctions are significantly more stable than J1. The T_m values of the hairpin four-way junctions are 25.2° to 32.2°C higher than the control, J1. With respect to protein recognition, gel shift assays reveal that the DNA-binding proteins HMGBb1 and HMGB1 bind the hairpin four-way junctions with affinity levels similar to control, J1. To evaluate nuclease resistance, four-way junctions are incubated with DNase I, exonuclease III (Exo III) and T5 exonuclease (T5 Exo). The enzymes probe nucleic acid cleavage that occurs non-specifically (DNase I) and in a 5′→3′ (T5 Exo) and 3′→5′ direction (Exo III). The nuclease digestion assays clearly show that the intramolecular four-way junctions possess significantly higher nuclease resistance than the control, J1.

Keywords: Intramolecular DNA junctions, four-way junctions, HMGB1, phosphorothioate bonds, nuclease resistance, DNA hairpins

***Experimental Biology and Medicine* 2021; 246: 707–717. DOI: 10.1177/1535370220973970**

Introduction

In principle, nucleic acid-based therapeutics afford high binding specificity, ease of synthesis and low toxicity.[1] Reports show that nucleic acids can be directed against target proteins such as the highly abundant DNA-binding cytokine, high mobility group B1 (HMGB1). In earlier studies, single-strand DNA composed of phosphorothioate (PS) bonds, bent duplex and DNA four-way junctions (4WJs) have been used to target HMGB1.[2–4] HMGB1 was initially identified as an exceptionally abundant architectural nuclear protein.[5] In the nucleus, HMGB1 binds the minor groove of bent/distorted DNA with high affinity to promote vital cellular processes such as chromatin remodeling and DNA recombination and repair.[6,7] More recent studies reveal that

HMGB1 also functions as a redox-sensitive damage-associated molecular pattern (DAMP) molecule.[8] In this capacity, HMGB1 binds immune receptors including: CXR4 (via the HMGB1:CXCL12 complex), RAGE, and TLR-2,4 to initiate leukocyte migration and pro-inflammatory gene expression.[9–11] Moreover, several independent studies link deleterious HMGB1 proinflammatory signaling with diseases and immune disorders ranging from atherosclerosis, cancer, cystic fibrosis and lupus to rheumatoid arthritis and sepsis.[12]

We hypothesize that nucleic acid constructs based on the classic immobilized four-way junction, J1, can be developed as high affinity ligands against HMGB1. J1 is assembled from four asymmetric DNA strands.[13] Strand asymmetry ensures that the junction branch point is immobilized. Biophysical studies have identified two distinct structural states of immobilized 4WJs: (i) an open-x and (ii) a stacked-x conformer (Figure 1(a)). In low ionic strength solutions (<100 μM Mg^{2+}), the open-x conformer is favored.[14,15] In high ionic strength solutions (>100 μM Mg^{2+}), the duplex arms of the open-x conformer stack coaxially to generate two potential structural isomers (stacked-x I/II and III/IV). Hydroxyl radical footprinting, NMR and FRET experiments show that J1 favors the I/II stacked conformer in high Mg^{2+}.[16,17]

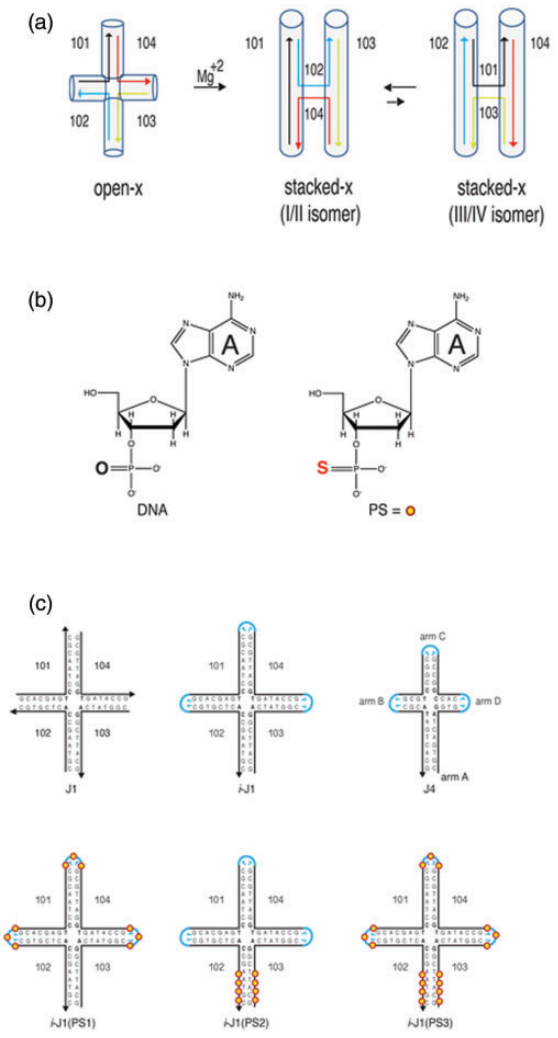

Figure 1. (a) Graphical models of open-x and stacked-x conformational isomers of the immobilized junction, J1; (b) monomer of natural vs. phosphorothioate (PS) DNA; (c) schematic of the intramolecular 4WJs: J1, *i*-J1, J4, *i*-J1(PS1), *i*-J1(PS2) and *i*-J1(PS3). PS bonds highlighted with red and yellow icons. (A color version of this figure is available in the online journal.)

In efforts to increase the thermostability and nuclease resistance of J1 for *ex vivo* HMGB1 targeting experiments, H2-type mini-hairpins are inserted at three helical termini of J1 to generate a species that we designate *i*-J1. A schematic of *i*-J1 is displayed in Figure 1(c). The H2-type hairpins reduce conformational entropy within the junction arms and reduce end fraying; both factors enhance thermostability. A similar strategy was used to generate the smaller intramolecular DNA junction J4 (Figure 1(c)).[18] More recently, Carr *et al*. designed a thermostable intramolecular 4WJ that contains hairpins composed of five consecutive thymine residues.[19] We hypothesize that the mini-hairpins will also enhance resistance against exonucleases at least in part by effectively removing binding sites (e.g. free 3′ and 5′-ends). To further increase nuclease resistance, phosphorothioate bonds (PS) are inserted into the hairpin regions and the double stranded "stem" of *i*-J1. PS bonds replace a non-bridging oxygen atom with a sulfur in the backbone of the oligonucleotide. A schematic of a DNA vs. PS monomer is displayed in Figure 1(b). Reports show that oligonucleotides containing PS bonds possess enhanced nuclease resistance vs. DNA and RNA homologs.[20,21] Here, we designate the three resulting PS intramolecular 4WJs as shown in Figure 1(c): *i*-J1(PS1), *i*-J1(PS2) and *i*-J1(PS3).

Each 4WJ is characterized by investigating the secondary structure using circular dichroism (CD). Next, the HMGB binding affinity is evaluated. The protein binding experiments focus on the recombinant HMG subunit protein, HMGB1b, and the full-length protein, HMGB1. HMGB1b is selected because this isolated protein subunit influences the transcription of proinflammatory genes.[22,23] A schematic of HMGB1 including the 3D structures of each box subunit (HMGB1a and HMGB1b) are shown in Figure 2.[24,25] Finally, the nuclease resistance of each junction is evaluated using three enzymes: DNase I, Exonuclease III (Exo III) and bacteriophage T5 Exonuclease (T5 Exo). These enzymes probe nucleic acid hydrolysis that occurs: non-specifically (DNase I), in a 3′→5′ direction (Exo III) and a 5′→3′ direction (T5 Exo). DNase I is an endonuclease that hydrolyzes double and single-strand DNA in a largely non-specific manner to generate mono- and oligodeoxyribonucleotides.[26,27] Exo III is the major apurinic/apyrimidinic DNA-repair enzyme in *E. coli*. Exo III can function as a: 3′→5′ exonuclease, 3′-repair diesterase, 3′-phosphomono-esterase and ribonuclease.[28] Here, we focus on the 3′→5′ exonuclease activity of the enzyme. DNase I and Exo III possess high structural homology, both enzymes have a four-layer α/β-sandwich fold, but < 20% sequence homology. Structural models indicate that DNase I and Exo III bind tightly within the minor groove of DNA.[29,30] T5 Exo is a polymerase-associated nuclease that can act as an endo- or exonuclease to hydrolyze ssDNA and dsDNA. T5 Exo hydrolysis generates mono-, di-, tri- and oligonucleotides.[31]

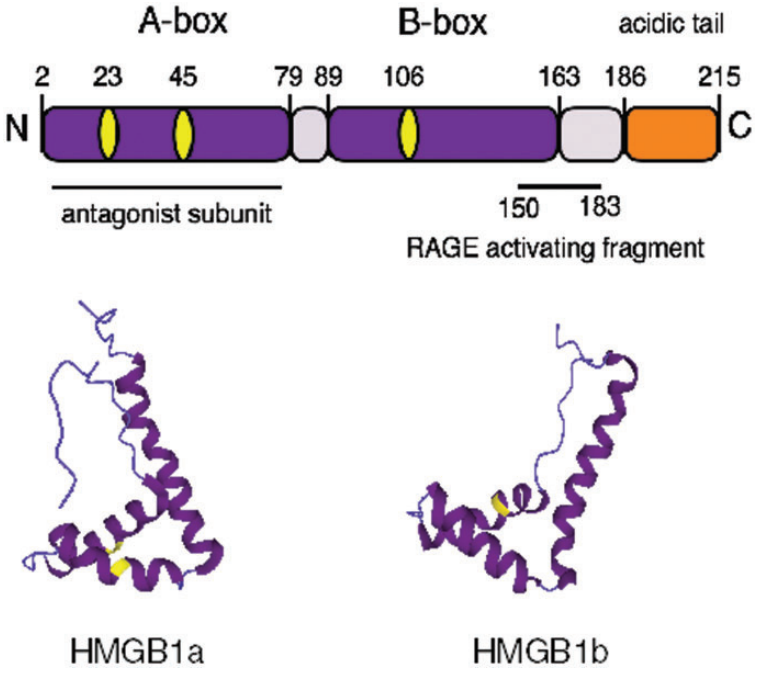

Figure 2. Schematic of HMGB1 and the 3D structure of the corresponding A- and B-box subunits. Each structure corresponds to the following PDB entries 2RTU and 1HME. (A color version of this figure is available in the online journal.)

CD studies indicate that the secondary structure of the intramolecular 4WJs, like J1, consists predominantly of B-form helices. CD thermal unfolding assays show that the thermostability of each intramolecular 4WJ is significantly higher than the control, J1. With respect to the protein binding assays, electrophoretic mobility shift assays (EMSAs) show that HMGB1 binds the each hairpin 4WJ with very high affinity. Finally, nuclease digestion studies reveal that the intramolecular junctions are significantly more resistant to nuclease hydrolysis vs. J1. We conclude that H2-type mini-hairpin junctions represent promising lead reagents capable of blocking the biological effects of HMGB1.

Materials and methods

Four-way junction oligonucleotides

The sequences for J1 are: 101, 5′-CGCAATCCTGAGCACG-3′; 102, 5′-CGTGCTCACCGAATGC-3′; 103, 5′-GCATTCG GACTATGGC-3′ and 104, 5′-GCCATAGTGGATTGCG. The J4 sequence is: 5′-GCACTGCTACGC**TT**GCGTCC GGC**TT**GCCGGCCAC**TT**GTGGAGCAGTGC-3′. The sequence for *i*-J1 is: 5′- CGTAAGCCACTCGTGC**TT** GCACGAGTCCTAACG C**TT**GCGTTAGGTGATACCG **TT**CGGTATCAGGCTTACG-3′. The sequence for *i*-J1(PS1) is: 5′- CGTAAGCCACTCGTGC***T*****T***GCACGAGTCCT AACG C***T*****T***GCGTTAGGTGATACCG***T*****T***CGGT ATCAGGCTTACG-3′. The sequence for *i*-J1(PS2) is: 5′-C*G*T*A*AGCCACTCGTGC**TT**GCACGAGTCCTAACG C**TT**GCGTTAGGTGATACCG**TT**CGGTATCAGGCT*T*A*C *G-3′. The sequence for *i*-J1(PS3) is: 5′-C*G*T*A*AGCCACTCGTGC***T*****T***GCACGAGTCCTAACG C***T*****T***GCGTTAGGTGATACCG***T*****T***CGGTATCAGGCT* T*A*C*G-3′. The hairpin regions of each junction are labeled in bold text. The PS bonds are denoted with asterisks. To detect each H2-type junction for gel analysis (Figures 3, 5 and 6), the 5′ end of each 4WJ is conjugated with fluorescein. For the intermolecular DNA control J1, the 5′ end of the single strand 101 is conjugated with fluorescein. All DNA strands are synthesized and purified (via HPLC) from Integrated DNA Technologies (IDT).

Preparation of 4WJs

J1 is formed by lyophilizing a mixture of a fluorescein-labeled strand (25 μM) with 5-fold excess of unlabeled strands (125 μM); 10 μL of fluorescein labeled 101 is mixed with 10 μL of each unlabeled strand 102, 103 and 104 and lyophilized. The pellet is suspended in 10 μL annealing buffer (50 mM Tris-HCl, 1.0 mM $MgCl_2$ (pH 7.5)), incubated at 95°C for 2 min and cooled to room temperature for 12–16 h. The final concentration of J1 (25 μM) is an approximation that is based on assuming complete conversion of the limiting strand (25 μM 101*) into a stable four-way junction. Each intramolecular junction is prepared by suspending lyophilized DNA with deionized nuclease-free water. Intramolecular junctions are subsequently diluted to 25 μM in annealing buffer. To determine the purity of 4WJs, each sample is loaded onto 15% mini-PROTEAN non-denaturing polyacrylamide gels (BioRad) and run at 10–15 mA for approximately 90 min at 4°C. The electrophoresis running buffer contains 0.5 × TBE•$MgCl_2$ (45 mM Trisma, 45 mM boric acid, 1.0 mM EDTA, 1 mM $MgCl_2$) at pH 7.6. The gels are subsequently scanned with a Gel Doc EZ Imager (BioRad).

Circular dichroism analysis

CD spectra are recorded using a Jasco J-815 spectrometer; 10.0 μM of each 4WJ are analyzed in CD run buffer (20 mM

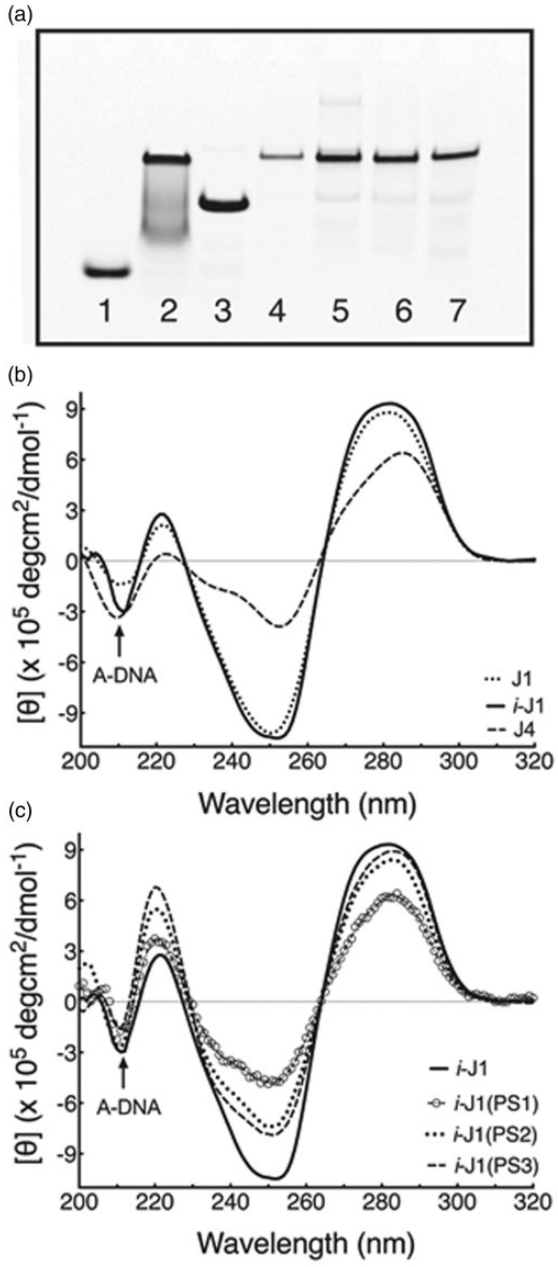

Figure 3. (a) Non-denaturing gel electrophoresis of 4WJs. Lane (1) 101, (2) J1, (3) J4, (4) *i*-J1, (5) *i*-J1(PS1), (6) *i*-J1(PS2) and (7) *i*-J1(PS3). (b) CD spectra of intramolecular DNA 4WJs: J1, *i*-J1 and J4. (c) CD spectra of intramolecular DNA-PS 4WJs: *i*-J1(PS1), *i*-J1(PS2) and *i*-J1(PS3) *vs.* *i*-J1. In each panel, the figure legend for each sample denotes the corresponding sample.

HEPES, 30 mM NH_4Cl, 200 mM KCl, 2 mM DTT, 1 mM $MgCl_2$, 10% glycerol at pH 7.4). All spectra are measured in a 0.1 cm path-length quartz cuvette. Each scan is recorded from 320 to 200 nm in 1.0 nm increments at 10°C. The CD spectra displayed in Figure 3 are based on three or more independent assays.

Circular dichroism denaturation assays

CD thermal denaturation scans of each junction are recorded by measuring the CD signal at a fixed wavelength (~280 nm) from 10° to 90°C in 2° increments. The thermal denaturation analysis buffer is identical to the buffer used

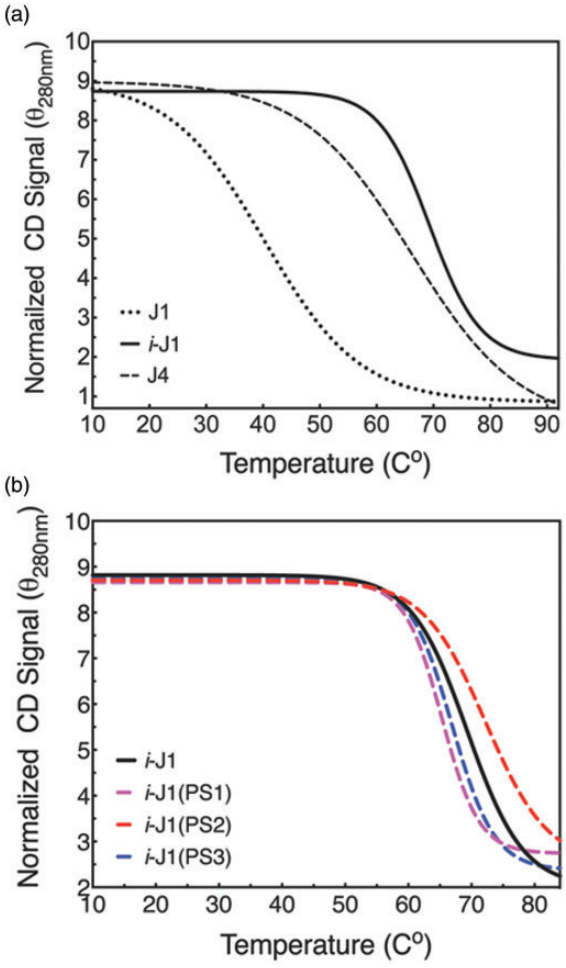

Figure 4. (a) CD thermal denaturation curves of intramolecular DNA 4WJs: J1, *i*-J1 and J4. (b) CD thermal denaturation curves of intramolecular DNA 4WJs: J1, *i*-J1 and J4. (c) CD spectra of intramolecular DNA-PS 4WJs: *i*-J1(PS1), *i*-J1(PS2) and *i*-J1(PS3) vs. *i*-J1. In each panel, the figure legend for each sample denotes the corresponding sample. (A color version of this figure is available in the online journal.)

in the CD scans. For J4 and *i*-J1(PS1), the starting concentration of each sample is increased to 15 μM to ensure the unfolding signal was on par with the other junctions analyzed. The melting temperature (T_m) value for each 4WJ is calculated by fitting the average value of three or more independent scans to a sigmoidal curve equation in GraphPad Prism. To ensure that the thermal unfolding data are on the same/similar scale, the averaged data are normalized by multiplying the data by 150 and the data were rescaled using the following equation: $x' = (x - x_{min})(10 - 1)/(x_{max} - x_{min})$.

Protein expression

Rat HMGB1b is produced from the pHB1 expression plasmid in *E. coli* Bl21(DE3) and purified according to the protocols described by Chow *et al*.[32] Rat HMGB1 is produced from a pET-16b expression plasmid using *Escherichia coli* Bl21(DE3) cells and purified using a standard His-tag purification protocol (GenScript). The rat version of both proteins is identical to the human ortholog. The purity of each protein sample is monitored by resolution on 12%

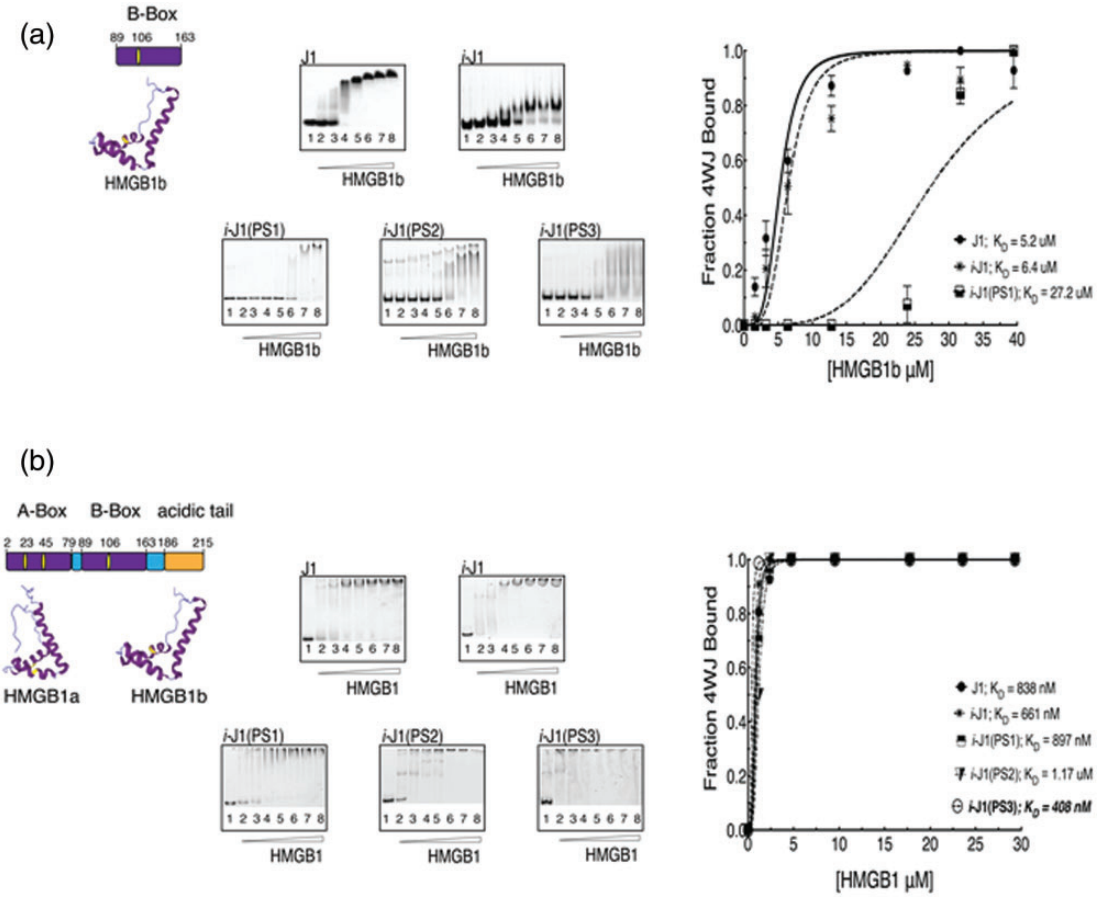

Figure 5. EMSA and the corresponding nonlinear fitting analysis of protein—4WJ junction binding. (a) For HMGB1b analysis, lane 1 of each gel contains the 0.5 μM of each 4WJ; lanes 2–8 represent 0.5 μM of each 4WJ incubated with HMGB1b at protein/4WJ ratios of: 3.2:1, 6.4:1, 12.8:1, 25.6:1, 47.8:1, 63.4:1 and 79:1. (a) For the HMGB1 analysis, lanes 2–8 represent 0.5 μM of each 4WJ incubated with HMGB1b at protein/4WJ ratios of: 2.4:1, 4.7:1, 9.5:1, 19.0:1, 35.5:1, 47.1:1 and 60.0:1. In each panel, the figure legend denotes the binding isotherm for each 4WJ and the corresponding binding constant (K_D). (A color version of this figure is available in the online journal.)

SDS-polyacrylamide gels. The resulting gel is stained for 12 h with Coomassie Brilliant Blue G-250.[33] The purity of HMGB1 and HMGB1b is confirmed by the presence of one predominant band at approximately 25 and 10 kDa (Supplemental Figure 1). The concentration of each protein is determined by methods previously described by Pace *et al*.[34]

Electrophoretic mobility shift assays

At 4°C, 500 nm of each junction is incubated with increasing concentrations of protein (HMGB1b or HMGB1) for 30 min in binding buffer [20 mM Tris-HCl (pH 7.5), 10 mM NaCl, 1 mM $MgCl_2$ and 10% (v/v) glycerol]. Lane 1 of the gels in Figure 5 corresponds to the 4WJ of interest, lanes 2–8 represent each 4WJ incubated with increasing amounts of protein. The protein and junction are expressed in terms of molar ratio of protein to junction (P/J). For the HMGB1b assays, lanes 2–8 represent 0.5 μM of each 4WJ incubated with HMGB1b at protein/4WJ ratios of: 3.2:1, 6.4:1, 12.8:1, 25.6:1, 47.8:1, 63.4:1 and 79:1. For the HMGB1 assays, lanes 2–8 represent 0.5 μM of each 4WJ incubated with HMGB1 at protein/4WJ ratios of: 2.4:1, 4.7:1, 9.5:1, 19.0:1, 35.5:1, 47.1:1 and 60.0:1. To measure binding, each sample is loaded onto a 15% non-denaturing polyacrylamide gel and run at 4°C for 6–8 h. The EMSA run buffer is composed of 0.5 X TBE, 1 mM $MgCl_2$ (pH 7.6). Each gel is scanned and quantified with a Gel Doc EZ Imager (BioRad). The gels in Figure 5 represent one of three or more independent EMSAs.

Measurement of protein binding affinity

The binding data are quantified by measuring the fraction of 4WJ bound (f_b) vs. protein concentration and fit via nonlinear regression according to the following equation

$$f_b = (K_A X)^4/[1 + (K_A X)^4]$$

in GraphPad Prism 8 using a 95% confidence interval. X represents the protein concentration and K_A is the association constant. The equation represents a fully cooperative Langmuir binding isotherm that accounts for 4:1 binding stoichiometry.[35,36] The dissociation constant (K_D) is the reciprocal of K_A. The binding constants are derived from three or more independent EMSAs. The goodness of fit (R^2) to the binding equation for HMGB1b binding to J1 and *i*-J1 are 0.8937 and 0.8552. The R^2 values for HMGB1 binding to

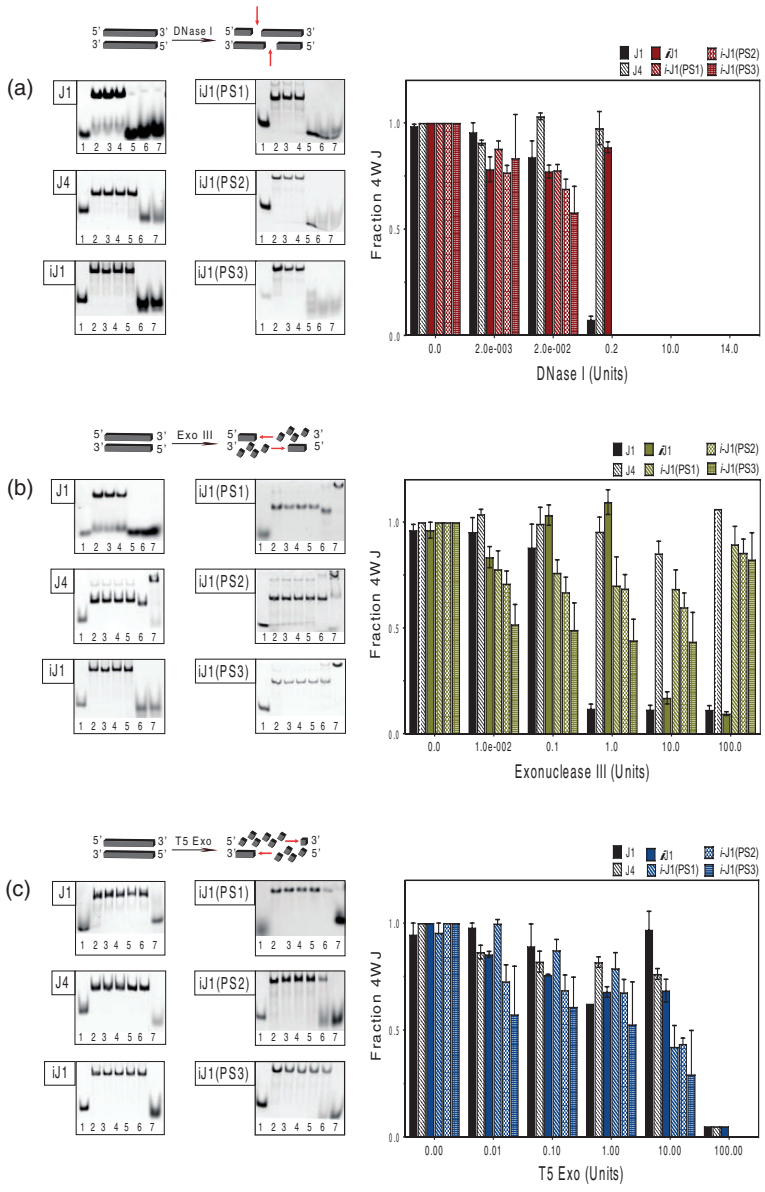

Figure 6. Nuclease resistance data. Non-denaturing gels for each 4WJ are displayed in the left column. Lane 1 contains 0.5 μM of ssDNA. Lane 2 of each gel contains 0.5 μM of each 4WJ in the absence of nuclease. Lanes 3–7 correspond to 0.5 μM of each 4WJ incubated in the presence of increasing nuclease. Panel (a) represents the remaining fraction of intact junction following digestion with: 0.0020, 0.020, 0.20, 10.0 and 14.0 units (lanes 3–7) of DNase I. Panel (b) represents the remaining fraction of intact junction following digestion with: 0.010, 0.10, 1.0, 10.0 and 100.0 units (lanes 3–7) of Exo III. Panel (c) represents the remaining fraction of intact junction following digestion with: 0.0010, 0.010, 0.10, 10.0 and 100.0 units (lanes 3–7) of T5 Exo. (A color version of this figure is available in the online journal.)

J1, *i*-J1, *i*-J1(PS1), *i*-J1(PS2) and *i*-J1(PS3) are: 0.9934, 0.9998, 0.9993, 0.9967 and 0.9997.

Nuclease resistance assays

Each DNA junction (500 nM) is incubated in the presence of DNase I, Exo III, or T5 Exo at 37°C. The DNase I reactions are quenched after 30 min; the Exo III and T5 Exo reactions are quenched after 10 min. All nuclease reactions are quenched with 80% glycerol (10% v/v final concentration) and immediately loaded onto 15% non-denaturing polyacrylamide gels. In each gel, lane 1 contains an ssDNA control (101*), lane 2 contains the 4WJ control and lanes 3–7 represent the junction of interest incubated with increasing nuclease. For the DNase I reactions, lanes 3–7 correspond to 0.0020, 0.020, 0.20, 10.0 and 14.0 units of enzyme. For the Exo III reactions, lanes 3–7 correspond to 0.010, 0.10, 1.0, 10.0 and 100.0 units of enzyme. For the T5 Exo digests, lanes 3–7 correspond to 0.0010, 0.010, 0.100, 10.0 and 100.0 units of enzyme. Each gel is run at 4°C in run buffer (0.5 X TBE, 1 mM $MgCl_2$ (pH 7.6)) for 90 min and scanned using a Gel Doc EZ Imager. The fraction of intact 4WJs is determined by dividing the number of counts of remaining 4WJ by the total number of counts in the control reaction (lane 2). The gels and corresponding bar graphs that indicate nuclease stability are dispalyed in Figure 6. Each data set represents three or more independent assays. All enzymes are purchased from New England Biolabs.

Results

Electrophoretic mobility of intramolecular four-way junctions

Non-denaturing polyacrylamide gel electrophoresis is used to compare the gross conformational features of each intramolecular junction vs. the control, J1. In Figure 3(a), lanes 1–7 correspond to the: the ssDNA control 101, J1, J4, *i*-J1, *i*-J1 (PS1), *i*-J1(PS2) and *i*-J1(PS3). As shown in lanes 4–7, each intramolecular junction migrates with the nearly identical mobility to the control, J1 (lane 2). The electrophoretic mobility of the smaller junction J4 (lane 3) is as expected intermediate between the ssDNA (lane 1) and the larger 4WJs. The faint high mobility bands present in the control, J1 (lane 2) indicate that J1 dissociates slightly during gel analysis. In our prior studies, rigorous controls were conducted to confirm that the high mobility bands did not assemble to form a contaminating "J1-like" structure.[37,38]

Circular dichroism analysis

The CD spectra of DNA 4WJs have signature minimum and maximum bands at 250 and 280 nm that correspond to B-form helices.[39–42] The CD spectrum of A-form DNA resembles that of RNA. Both A-form DNA and RNA CD spectra have prominent minima and maxima at 210 and 260 nm. Studies show that the CD spectra of certain triplex DNA structures can also possess a minimum at ~210 nm.[43–45] For clarity, the CD spectra of the natural DNA 4WJs (J1, *i*-J1 and J4) are displayed in Figure 3(b) and the PS containing 4WJs are shown in Figure 3(c). In Figure 3(b), the CD spectra of J1 (dashed black line) generate prominent B-form bands at 250 and 280 nm as expected. Like the control, *i*-J1 (solid black line) also displays strong B-form bands. However, *i*-J1 possesses a larger signal at 210 nm vs. J1. Like *i*-J1, J4 (dotted line) also displays a relatively stronger signal at 210 nm vs. J1. J4 generates a lower CD signal presumably due to reduced level of base stacking within the smaller junction lattice. In Figure 3(c), a direct comparison of the PS-4WJs reveals that the two junctions that contain PS bonds in the stem region (e.g. *i*-J1(PS2) and *i*-J1(PS3)) display enhanced B-form signals at 280 nm. *i*-J1(PS1) generates a similar CD spectra but the magnitude of the signal is relatively lower than the other PS constructs. Like *i*-J1, the PS 4WJs contain relatively stronger signals at 210 nm vs. J1. Based on the stringent sequence restriction of the immobilized 4WJ lattice, logic suggests the CD minima at 210 nm correspond to A-form DNA. However, higher resolution techniques are required to confirm that small populations of triplex or triplex-like structures are not present. Each CD scan is based on the average of three or more independent runs.

Next, thermal denaturation scans are conducted to provide an estimate of the conformational stability of each intramolecular junction vs. the control, J1. The stability of each junction is determined by measuring the reduction in helical content at 280 nm. Figure 4(a) displays the melting curves for J1, *i*-J1 and J4; the PS containing 4WJs vs. *i*-J1 are shown in Figure 4(b). The T_m of the control J1 is 40.1°C. Each intramolecular junction has a significantly higher T_m vs. J1; the T_m values range from 25.2° to 32.2°C. A comparison of the thermal denaturation curves in Figure 4 reveals a stability ranking of: *i*-J1(PS2)>*i*-J1> *i*-J1(PS3)> J4>*i*-J1(PS1)⋙J1. The T_m and ΔT_m values for each junction are listed in Table 1. The shape of each unfolding curve represents a monophasic transition from the folded to the unfolded state. We suspect that the lack of intermediate structures is due to the presence of high concentrations of Mg^{2+} in the analysis buffer. Similar unfolding trends are also noted in the intramolecular 4WJs in high ionic strength buffers. In those studies, intermediate species/conformers are present at low salt conditions but shift to one predominant folded species upon shifting to high ionic strength buffer.[19,46] The thermal denaturation data in Figure 4 is based on the average of three or more independent scans.

Table 1. Thermal unfolding temperature of intramolecular 4WJs vs. J1.

Junction	T_m (°C)	ΔT_m (°C)
J1	40.1	
i-J1	69.3	29.2
i-J1(PS1)	65.3	25.2
i-J1(PS2)	72.3	32.2
i-J1(PS3)	66.9	26.8

EMSA analysis of HMG protein binding toward intramolecular 4WJs

EMSAs are used to evaluate the binding affinity of the recombinant DNA binding protein HMGB1b and the full-length protein, HMGB1, toward intramolecular 4WJs. Xin *et al.* used: analytical ultracentrifugation, fluorescence and EMSA analyses to show that HMGB1b binds J1 with a stoichiometry of four to one (4:1).[35] A tight 4:1 complex typically migrates as a single band without intermediate binding species. Previous data show that the full-length protein, HMGB1, also binds 4WJs with 4:1 binding stoichiometry.[47]

The EMSA data are displayed in Figure 5. In each gel, lane 1 contains the junction control (without protein); lanes 2–8 report on the mobility of each 4WJ in the presence of increasing amounts of protein. The protein and junction are expressed in terms of molar ratio of protein to junction (P/J). As shown in Figure 5(a), HMGB1b binds J1 with moderate affinity. Complete binding of HMGB1b to J1 is achieved upon increasing the P/J ratio to 6.4:1 (lane 4). HMGB1b binds *i*-J1 with a similar affinity profile to J1 but the electrophoretic mobility of the protein nucleic acid complexes is considerably smaller. HMGB1b displays initial weak binding interactions toward *i*-J1 at a P/J molar ratio of 6.4:1 (lane 4). Complete binding of HMGB1b to *i*-J1 occurs at 47.8:1 (lane 6). Gel shifts for HMGB1b and the PS 4WJs indicate that the protein binds these substrates with relatively lower affinity. Here, the formation of nucleic acid complexes occurs at higher P/J ratios (e.g. 63.4:1 (lane 7)) of HMGB1b. For these substrates, it is difficult to detect discrete 4:1 protein nucleic acid complexes. However, the absence of free 4WJ bands indicates that HMGB1b strongly binds to *i*-J1(PS2) and *i*-J1(PS3).

Next, the binding properties of the full-length protein, HMGB1, are investigated. For each junction, HMGB1 forms

a discrete complex at low P/J molar ratios (e.g. 2.37:1 (lane3)). The gels in Figure 5(b) display a binding pattern that is consistent with these results.

Summary of protein – 4WJ binding data

To calculate the apparent binding constants of HMGB1b and HMGB1 toward each junction, the EMSA data are fit to a modified Langmuir binding isotherm that describes 4:1 binding stoichiometry. The binding data for each junction are shown in the graphs in Figure 5; the y-axis displays the fraction of 4WJ bound (e.g. 4:1 complex) vs. protein concentration (x-axis). As shown in Figure 5(a), HMGB1b possesses the highest binding affinity toward the control J1 followed closely by *i*-J1. The apparent binding constants (K_Ds) for J1 and *i*-J1 are 5.2 μM and 6.4 μM. As stated earlier, HMGB1b possesses a relatively lower binding affinity trend toward the PS containing 4WJs. HMGB1b binds *i*-J1 (PS1) to generate a slightly larger K_D value of 27.2 μM. As stated earlier, it is not possible to accurately identity a stable 4:1 complex for HMGB1b with *i*-J1(PS2) and *i*-J1(PS3). Hence, we cannot reliably fit these substrates to the binding equation.

For HMGB1, the binding curves indicate that the full-length protein binds each 4WJ with significantly higher affinity. HMGB1 binds *i*-J1 and *i*-J1(PS3) with highest affinity; with K_D values of 661 nM and 408 nM. The K_D values for these substrates approach the reported binding constants for HMGB1 toward bent/cruciform DNA.[48–50] The binding constants for the remaining substrates indicate a relatively lower binding affinity profile; with K_D values of 838 nM for (J1); 897 nM for *i*-J1(PS1) and 1.17 μM *i*-J1(PS2).

Four-way junction nuclease resistance assays

DNase I, Exo III, and T5 Exo are used to investigate resistance of each junction against nonspecific cleavage (DNase I) and cleavage in either a 3′–5′ (Exo III) or 5′–3′ (T5 Exo) direction. The cleavage patterns for each nuclease are included above the gel images in Figure 6. In each gel, lane 1 contains an ssDNA control; lane 2 contains the 4WJ control and lanes 3–7 evaluate the resistance of each junction in the presence of increasing units of nuclease. An estimate of the nuclease resistance for each junction is displayed in the bar graph(s). The y-axis represents the fraction of intact junction at each nuclease concentration (x-axis). DNase I, Exo III, and T5 Exo data are shown in panels A, B and C. The data for the control J1 are displayed in black bars in each graph.

As shown in Figure 6(a), the control J1 is digested completely in the presence of 0.2 units of DNase I (lane 5). A direct comparison of the DNase I reactions indicates that *i*-J1 possesses the highest resistance values of all junctions tested. In the presence of 0.2 units of DNase I (lane 5), *i*-J1 remains intact, whereas the PS containing 4WJs (and the control) dissociate. *i*-J1 is completely digested in the presence of ≥ 10.0 units of DNase I (lanes 6–7). The accompanying bar graph clearly shows the level(s) of intact *i*-J1 (solid red bars) far exceeds those for J1 and the PS 4WJs.

Figure 6(b) summarizes the gel and resistance data for the Exo III digests. The control J1 is stable in the presence of lower amounts of Exo III (lanes 3 (0.01 units) and 4 (0.1 units)). However, moderate to high levels of Exo III completely digest the control [lanes 5–7 (≥ 1.0 units)]. A comparison of the stability of the intramolecular junctions shows that in each case the modified 4WJs possess higher stability in the presence of Exo III vs. the control. For *i*-J1, the junction remains intact in the presence of moderate Exo III (lane 5) but higher levels of Exo III (lanes 6–7) completely digest *i*-J1. The PS containing junctions display the largest increase in stability. In each case, the PS junctions appear to be inert to Exo III as evidenced by the lack of faster running bands that represent complete/high levels of hydrolysis. The bar graphs and gels both show that all the intramolecular junctions remain intact in the presence of excess Exo III (100 units (lane 7)). Somewhat surprisingly, there is a decrease in fluorescence counts for the PS intramolecular 4WJ in lanes 4–6. Although there is a reduction in the number of counts, the absence of cleaved species indicates that the PS junctions are resistant to Exo III.

The T5 Exo data are displayed in Figure 6(c). In this case, the control J1 is more stable in the presence of high levels of nuclease—as reflected by the intact bands in lane 6 (10.0 units). Extremely high levels of T5 Exo completely dissociate J1 (lane 7 (100.0 units). The gels for the intramolecular 4WJs show a similar nuclease stability profile, in that the 4WJs remain largely intact in the presence of high levels of nuclease as shown in lanes 3–6 (≤ 10.0 units T5 Exo). The bar graph data reveal a stability profile of: J1>*i*-J1>*i*-J1 (PS1)>*i*-J1(PS2)>*i*-J1(PS3). The gels and the corresponding bar graphs are based on at least three independent digests per nuclease. The data clearly show that each nuclease digests the intact 4WJs to smaller species that migrate with a similar mobility to the ssDNA control. In each case, smaller cleavage products (e.g. oligonucleotide fragments) should be observed that migrate faster than the ssDNA control. We suspect the lack of faster running species is due to the high concentration of Mg^{2+} in the run buffer that may reduce the cleavage of the DNA strands.

Discussion

Our research objective is to assess the structure and protein recognition features of the intramolecular 4WJs. Non-denaturing gel analysis shows that all of the intramolecular junctions investigated possess nearly identical mobility to the control J1 (Figure 3(a)). The data indicate that the insertion of: (i) DNA H2-type mini-hairpins, (ii) PS bond H2-type hairpins and (iii) PS bonds in the junction stem do not appreciably alter the nucleic acid global fold of J1.

The CD studies show that intramolecular junctions have similar yet distinct spectra that imply potential differences in secondary structure. Each junction investigated possesses a strong/distinct B-form DNA band at 280 nm that is consistent with DNA 4WJ junctions.[39–42] The B-form band at 250 nm for J1 and *i*-J1 is also quite strong. For the PS 4WJs, the amplitude of the band at 250 nm is considerably lower. Moreover, the band at 220 nm for the PS 4WJs displays a concomitant increase that is not as pronounced in the spectra for J1 and *i*-J1. Vorlickova *et al*. use CD to measure the structural differences between hairpin forming

trinucleotide repeats vs. non-hairpin forming controls (e.g. duplex anti-parallel DNA repeats).[51] In their work, the CD spectra of hairpin trinucleotide repeats display: (i) strong B-form maxima at 280 nm, (ii) weaker/diminished B-form DNA bands at 250 nm and (iii) a band with increasing amplitude at 220 nm vs. the control.[51] Using this data, it is tempting to hypothesize that the CD spectra of the PS 4WJs possess increased levels of hairpin structure. However, high resolution techniques are required to test this hypothesis.

The thermal denaturation scans confirm that the stability of J1 can be enhanced significantly by inserting hairpins (natural and PS containing). The ΔT_m values of the intramolecular 4WJs range from 25.2° to 32.2°C. The increase in stability is likely due to reduced end fraying and conformational flexibility.

With respect to the protein binding characteristics of intramolecular 4WJs, the full length protein HMGB1 binds certain constructs [*i*-J1 and *i*-J1(PS3)] with K_D values slightly above previously reported values. Based on these data, it appears that the overall structural fold of the intramolecular junctions provides a favorable protein binding platform. HMGB1 binds intramolecular 4WJs with much higher affinity than the single subunit, HMGB1b. For HMGB1b, the estimated K_D values are on the μM scale. Prior binding studies of isolated HMG subunits (e.g. HMGB1a and HMGB1b) estimated K_D values on the nM scale.[35] We hypothesize that the reduction in HMGB1b binding affinity is due at least in part to the presence of high Mg^{2+} (1 mM) in the binding and analysis buffer. Research by Pohler *et al*. clearly shows that the binding affinity of the single subunit HMGB1a toward 4WJs is inversely proportional to Mg^{2+} concentration.[52] In our case, the Mg^{2+} concentration is increased to 1 mM to reduce the dissociation of the control, J1. It is plausible that the Mg^{2+} ions effectively screen the phosphate backbone of the DNA to reduce protein binding. However, it is clear that high Mg^{2+} does not reduce the binding affinity of the full length protein, HMGB1 toward cruciform/bent DNA. The binding behavior of HMGB1 is not surprising because 1 mM is at/near physiological conditions.[53]

Figure 5(a) also shows that, HMGB1b somewhat surprisingly does not form discrete 4:1 complexes with *i*-J1(PS2) and *i*-J1(PS3). This result could be due to the presence of PS bonds in both strands of the stem region of each 4WJ. It is plausible that sulfur atoms alter the minor groove topology near the protein binding region such that discreet 4:1 complexes do not form. High resolution structural data or analytical ultracentrifugation experiments are required to support this. It is also plausible that the presence of the PS bonds in close proximity to the fluorophore results in self-quenching of the signal—as a result the number of counts of the 4:1 complex are not prominent and thus effectively masked in the smeared band(s).

The nuclease resistance data reveal that the insertion of: (i) DNA H2-type mini-hairpins, (ii) PS bond H2-type hairpins and (iii) PS bonds in the junction stem effectively enhance the stability of 4WJs vs. DNase I (endonuclease) and Exo III (3′–5′ exonuclease). The DNase I studies reveal that *i*-J1 is clearly the most stable 4WJ investigated. It is somewhat surprising that the phosphorothioate bonds of the PS junctions do not generate a concomitant increase in stability. One potential explanation may be linked to the reduction in B-form CD signal at 250 nm. As stated earlier, we hypothesize that this spectral phenomenon may represent an increase in hairpin structure. It is plausible that the stabilized hairpins introduce or enhance local perturbations within the duplex arms that permit greater access to the minor groove. Again, high resolution analysis is required to confirm this hypothesis. The Exo III digests show that the intramolecular 4WJs are significantly more stable than J1. The bar graph data (Figure 6(b)) reveal a stability order of: *i*-J1(PS1) > *i*-J1(PS2) > *i*-J1(PS3) > *i*-J1 ≫ J1. The increase in 3′ nuclease stability of the intramolecular 4WJs vs. J1 may be the result of effectively removing the free 3′ end (via end-capping) that in turn reduces exonuclease activity. One could also speculate that the high resistance values, for the PS 4WJs, may be attributed to stabilized hairpin regions that prevent cleavage via Exo III. Again, high resolution structural analysis is required to provide more detailed information to confirm this.

Conclusions

We have constructed and characterized important properties of four new intramolecular DNA junctions. Our data indicate that the intramolecular constructs have substantially improved potential to serve as reagents for *in vivo* suppression of HMGB1 activity. Whereas the intermolecular junction J1 dissociates at moderate temperature(s) and is vulnerable to nuclease attack, the intramolecular analogs are significantly more stable and nuclease resistant. We await additional experimental data describing the role of these new reagents *in vivo*.

AUTHORS' CONTRIBUTIONS

All authors conducted experiments and participated in the analysis of data and AJB wrote the manuscript.

ACKNOWLEDGMENTS

The authors thank Dr. Neville R. Kallenbach and Dr. Matthew C.T. Hartman for advice.

DECLARATION OF CONFLICTING INTERESTS

The author(s) declared no potential conflicts of interest with respect to the research, authorship, and/or publication of this article.

FUNDING

The author(s) disclosed receipt of the following financial support for the research, authorship, and/or publication of this article: The research received funding from the University of San Diego.

ORCID ID

Anthony J Bell https://orcid.org/0000-0003-3813-9043

SUPPLEMENTAL MATERIAL

Supplemental material for this article is available online.

REFERENCES

1. Zhu G, Chen X. Aptamer-based targeted therapy. *Adv Drug Deliv Rev* 2018;**134**:65–78
2. Yanai H, Chiba S, Ban T, Nakaima Y, Onoe T, Honda K, Ohdan H, Taniguchi T. Suppression of immune responses by nonimmunogenic oligodeoxynucleotides with high affinity for high-mobility group box proteins (HMGBs). *Proc Natl Acad Sci U S A* 2011;**108**:11542–7
3. Musumeci D, Bucci EM, Roviello GN, Sapio R, Valente M, Moccia M, Bianchi ME, Pedone C. DNA-based strategies for blocking HMGB1 cytokine activity: design, synthesis and preliminary in vitro/in vivo assays of DNA and DNA-like duplexes. *Mol BioSyst* 2011;**7**:1742–52
4. Ju Z, Chavan SS, Antoine DJ, Dancho M, Tsaava T, Li J, Lu B, Levine YA, Stiegler A, Tamari Y, Al-Abed Y, Roth J, Tracey KJ, Yang H. Sequestering HMGB1 via DNA-conjugated beads ameliorates murine colitis. *PLoS One* 2014;**9**:e103992
5. Bustin M, Reeves R. High-mobility-group chromosomal proteins: architectural components that facilitate chromatin function. *Prog Nucleic Acid Res Mol Biol* 1996;**54**:35–100
6. Agresti A, Bianchi ME. HMGB proteins and gene expression. *Curr Opin Genet Dev* 2003;**13**:170–8
7. Lange SS, Vasquez KM. HMGB1: the jack-of-all-trades protein is a master DNA repair mechanic. *Mol Carcinog* 2009;**48**:571–80
8. Deng M, Scott MJ, Fan J, Billiar TR. Location is the key to function: HMGB1 in sepsis and trauma-induced inflammation. *J Leukoc Biol* 2019;**106**:161–9
9. De Leo F, Quilici G, Tirone M, De Marchis F, Mannella V, Zucchelli C, Preti A, Gori A, Casalgrandi M, Mezzapelle R, Bianchi ME, Musco G. Diflunisal targets the HMGB1/CXCL12 heterocomplex and blocks immune cell recruitment. *EMBO Rep* 2019;**20**:e47788
10. Venereau E, Schiraldi M, Uguccioni M, Bianchi ME. HMGB1 and leukocyte migration during trauma and sterile inflammation. *Mol Immunol* 2013;**55**:76–82
11. Andersson U, Yang H, Harris H. High-mobility group box 1 protein (HMGB1) operates as an alarmin outside as well as inside cell. *Semin Immunol* 2018;**38**:40–8
12. Kang R, Chen R, Zhang Q, Hou W, Wu S, Cao L, Huang J, Yu Y, Fan XG, Yan Z, Sun X, Wang H, Wang Q, Tsung A, Billiar TR, Zeh HJ 3rd, Lotze MT, Tang D. HMGB1 in health and disease. *Mol Aspects Med* 2014;**40**:1–116
13. Seeman NC, Kallenbach NR. Design of immobile nucleic acid junctions. *Biophys J* 1983;**44**:201–9
14. Ortiz-Lombardia M, Eritja GR, Aymami J, Azorin F, Coll M. Crystal structure of a DNA Holliday junction. *Nat Struct Biol* 1999;**6**:913–7
15. Lilley DMJ. Structures of helical junctions in nucleic acids. *Q Rev Biophys* 2000;**33**:109–59
16. Churchill ME, Tullius TD, Kallenbach NR, Seeman NC. A Holliday recombination intermediate is twofold symmetric. *Proc Natl Acad Sci U S A* 1988;**85**:4653–6
17. Miick SM, Fee RS, Millar DP, Chazin WJ. Crossover isomer bias is the primary sequence-dependent property of immobilized Holliday junctions. *Proc Natl Acad Sci U S A* 1997;**94**:9080–4
18. Pikkemaat JA, van den Elst H, van Boom JH, Altona C. NMR studies and conformational analysis of a DNA four-way junction formed in a linear synthetic oligonucleotide. *Biochemistry* 1994;**33**:14896–07
19. Carr CE, Marky LA. Melting behavior of a DNA four-way junction using spectroscopic and calorimetric techniques. *J Am Chem Soc* 2017;**139**:14443–55
20. Smith CIE, Zain R. Therapeutic oligonucleotides: state of the art. *Annu Rev Pharmacol Toxicol* 2018;**59**:605–30
21. Yang H, Lundback P, Ottossson L, Erlandsson-Harris H, Venereau E, Bianchi ME, Al-Abed Y, Andersson U, Tracey KJ, Antoine DJ. *Mol Med* 2012;**18**:250–9
22. Youn JH, Kwak MS, Wu J, Kim ES, Ji Y, Min HJ, Yoo JH, Choi JE, Cho HS, Shin JS. Identification of lipopolysaccharide-binding peptide regions within HMGB1 and their effects on subclinical endotoxemia in a mouse model. *Eur J Immunol* 2011;**41**:2753–62
23. Li J, Kokkola R, Tabibzadeh S, Yang R, Ochani M, Qiang X, Harris HE, Czura CJ, Wang H, Ulloa L, Wang H, Warren HS, Moldawer LL, Fink MP, Andersson U, Tracey KJ, Yang H. Structural Basis for the proinflammatory cytokine activity of high mobility group box 1. *Mol Med* 2003;**9**:37–45
24. Wang J, Tochio N, Takeuchi A, Uewaki J, Kogayashi N, Tate S. Redox-sensitive structural change in the A-domain of HMGB1 and its implication for the binding to cisplatin modified DNA. *Biochem Biophys Res Commun* 2013;**441**:701–6
25. Weir HM, Kraulis PJ, Hill CS, Raine AR, Laue ED, Thomas JO. Structure of the HMG box motif in the B-domain of HMG1. *EMBO J* 1993;**12**:1311–9
26. Parsiegla G, Noguere C, Santell L, Lazarus RA, Bourne Y. The structure of human DNase I bound to magnesium and phosphate ions points to a catalytic mechanism common to members of the DNase I-like superfamily. *Biochemistry* 2012;**51**:10250–8
27. Junowicz E, Spencer JH. Studies on bovine pancreatic deoxyribonucleae A. I. General properties and activation with different bivalent metals. *Biochim Biophys Acta* 1973;**12**:72–84
28. Demple B, Herman T, Chen DS. Cloning and expression of APE, the cDNA encoding the major apurinic endonuclease: definition of a family of DNA repair enzymes. *Proc Natl Acad Sci U S A* 1991;**88**:11450–4
29. Suck D. DNA recognition by structure-selective nucleases. *Biopolymers* 1997;**44**:405–21
30. Mol CD, Kuo CF, Thayer MM, Cunningham RP, Tainer JA. Structure and function of the multifunctional DNA repair enzyme exonuclease III. *Nature* 1995;**374**:381–6
31. Pickering TJ, Garforth SJ, Thorpe SJ, Sayers JR, Grasby JA. A single cleavage assay for T5 5″–>3″ exonuclease: determination of the catalytic parameters for wild-type and mutant proteins. *Nucleic Acids Res* 1999;**27**:730–5
32. Chow CS, Barnes CM, Lippard SJ. A single HMG domain in high-mobility group 1 protein binds to DNAs as small as 20 base pairs containing the major cisplatin adduct. *Biochemistry* 1995;**34**:2956–64
33. Schägger H, von Jagow G. Tricine-sodium dodecyl sulfate-polyacrylamide gel electrophoresis for the separation of proteins in the range from 1 to 100 kDa. *Anal Biochem* 1987;**166**:368–79
34. Pace CN, Vajdos F, Fee L, Grimsley G, Gray T. How to measure and predict the molar absorption coefficient of a protein. *Protein Sci* 1995;**4**:2411–23
35. Xin H, Taudte S, Kallenbach NR, Limbach MP, Zitomer RS. DNA binding by single HMG box model proteins. *Nucleic Acids Res* 2000;**28**:4044–50
36. Totsingan F, Bell AJ. Jr, Interaction of HMG proteins and H1 with hybrid PNA-DNA junctions. *Protein Sci* 2013;**22**:1552–62
37. Iverson D, Serrano C, Brahan AM, Shams A, Totsingan F, Bell AJ. Jr, Supporting data for the characterization of PNA–DNA four-way junctions. *Data Brief* 2015;**5**:756–60
38. Iverson D, Serrano C, Brahan AM, Shams A, Totsingan F, Bell AJ. Jr, Characterization of the structural and protein recognition properties of hybrid PNA–DNA four-way junctions. *Arch Biochem Biophys* 2015;**587**:1–11
39. Zhang W, Wu Q, Pwee K-H, Jois SDS, Kini RM. Characterization of the interaction of wheat HMGa with linear and four-way junction DNAs. *Biochemistry* 2003;**42**:6596–07
40. Howell LA, Waller ZAE, Bowater R, O'Connell M, Searcey M. A small molecule that induces assembly of a four way DNA junction at low temperature. *Chem Commun* 2011;**47**:8262–4
41. Kypr J, Kejnovska I, Renciuk D, Vorlickova M. Circular dichroism and conformational polymorphism of DNA. *Nucleic Acids Res* 2009;**37**:1713–25
42. Ranjbar B, Gill P. Circular dichroism techniques: biomolecular and nanostructural analyses – a review. *Chem Biol Drug Des* 2009;**74**:101–20
43. Avino A, Frieden M, Morales JC, Garcia de la Torre B, Guimil Garcia R, Azorin F, Gelpi JL, Orozco M, Gonzalez C, Erifja R. Properties of triple

helices formed by parallel-stranded hairpins containing 8-aminopurines. *Nucleic Acids Res* 2002;**30**:2609–19
44. Glick GD. Design, synthesis, and analysis of conformationally constrained nucleic acids. *Biopolymers* 1998;**48**:83–96
45. del Mundo IMA, Zewail-Foote M, Kerwin SM, Vasquez KM. Alternative DNA structure formation in the mutagenic *c-MYC* promoter. *Nucleic Acids Res* 2017;**45**:4929–43
46. Makube N, Klump HH. Impact of the third-strand orientation on the thermostability of the four-way DNA junction. *Arch Biochem Biophys* 2001;**393**:1–13
47. Taudte S, Xin H, Bell AJ, Jr, Kallenbach NR. Interactions between HMG boxes. *Protein Eng* 2001;**14**:1015–23
48. Hill DA, Reeves R. Competition between HMG-I(Y), HMG-1 and histone H1 on four-way junction DNA. *Nucleic Acids Res* 1997;**25**:3523–31
49. Pil PM, Lippard SJ. Specific binding of chromosomal protein HMG1 to DNA damaged by the anticancer drug cisplatin. *Science* 1992;**256**:234–7
50. Jung Y, Lippard SJ. Nature of full-length HMGB1 binding to cisplatin-modified DNA. *Biochemistry* 2003;**42**:2664–71
51. Vorlickova M, Kejnovska I, Bednarova K, Renciuk D, Kypr J. Circular dichroism spectroscopy of DNA: from duplexes to quadruplexes. *Chirality* 2012;**24**:691–8
52. Pohler JR, Norman DG, Bramham J, Bianchi ME, Lilley DM. HMG box proteins bind to four-way DNA junctions in their open conformation. *EMBO J* 1998;**17**:817–26
53. Romani A. Regulation of magnesium homeostasis and transport in mammalian cells. *Arch Biochem Biophys* 2007;**458**:90–102

(Received August 12, 2020, Accepted October 26, 2020)